New Journal of Physics
The open access journal for physics

The critical role of next-nearest-neighbor interlayer interaction in the magnetic behavior of magnetic/non-magnetic multilayers

Sunjae Chung[1], Sangyeop Lee[1], Taehee Yoo[1], Hakjoon Lee[1], J-H Chung[1], M S Choi[1], Sanghoon Lee[1,5], X Liu[2], J K Furdyna[2], Jae-Ho Han[3], Hyun-Woo Lee[3] and Kyung-Jin Lee[4]

[1] Department of Physics, Korea University, Seoul 136-701, Korea
[2] Department of Physics, University of Notre Dame, Notre Dame, IN 46556, USA
[3] PCTP and Department of Physics, Pohang University of Science and Technology, Pohang, Kyungbuk 790-784, Korea
[4] Department of Materials Science and Engineering, Korea University, Seoul 136-701, Korea
E-mail: slee3@korea.ac.kr

New Journal of Physics **15** (2013) 123025 (11pp)
Received 21 August 2013, revised 15 November 2013
Accepted for publication 20 November 2013
Published 13 December 2013
Online at http://www.njp.org/
doi:10.1088/1367-2630/15/12/123025

Abstract. A striking multiple-step behavior has been observed in magneto-resistance measurements during magnetization reversal in anti-ferromagnetically coupled GaMnAs/GaAs:Be multilayers. This behavior arises from the splitting of the energy degeneracy of spin configurations established by nearest-neighbor interlayer exchange coupling (NN IEC) with contribution from the next-nearest-neighbor (NNN) IEC. This observation reveals that NNN IEC plays a crucial role in the magnetic behavior of these multilayer structures.

[5] Author to whom any correspondence should be addressed.

Content from this work may be used under the terms of the Creative Commons Attribution 3.0 licence. Any further distribution of this work must maintain attribution to the author(s) and the title of the work, journal citation and DOI.

© IOP Publishing Ltd and Deutsche Physikalische Gesellschaft

Contents

1. Introduction 2
2. Sample preparation 2
3. Results and discussion 3
4. Conclusions 9

Acknowledgments 10

References 10

1. Introduction

The interlayer exchange interaction [1] in magnetic multilayers gives rise to giant magnetoresistance (GMR) [2, 3] and may thus lead to new breakthroughs in spin electronics [4]. It is therefore important to understand the fundamental principles behind such exchange interaction and to investigate its physical behaviors under different circumstances. Indeed, many studies have already been carried out on the interlayer exchange interaction in multilayer systems with various ferromagnetic (FM) materials [5–9], ranging from the dependence of the interlayer coupling strength on structural parameters to the oscillation between FM and anti-ferromagnetic (AFM) coupling [1, 10, 11]. Furthermore, the '3D spintronics device concept' has very recently been demonstrated by controlling the strength of exchange coupling between the magnetic layers [12–14]. However, all of these previous studies focused only on nearest-neighbor (NN) interactions between the magnetic layers.

In this study we report a striking step-wise behavior in magnetoresistance (MR), which cannot be explained in the frame of any existing theories based only on NN coupling, thus providing clear evidence that next-nearest-neighbor (NNN) interactions are significant. We show below that NNN interaction is of critical importance in magnetic semiconductor multilayers, where the Fermi wavelength ($\sim$4 nm in our GaMnAs samples) is significantly longer than in metallic multilayers, becoming comparable to the width of the layers [15–21]. Our finding is also important in the context of device applications of magnetic multilayer systems. Namely, by engineering the relative strengths of the NN and the NNN interactions, the MR can be switched from one behavior to another that is completely different.

We note that the effect of NNN coupling is most pronounced when the interlayer exchange coupling (IEC) is AFM [22–25]. It has been established that the AFM IEC in GaMnAs-based systems can only be achieved in a very narrow parameter window of carrier concentrations and structural dimensions [19, 26–28]. In this study, we therefore focus on magnetization reversal observed in a $[\mathrm{GaMnAs/GaAs{:}Be}]_{10}$ multilayer with GaMnAs and GaAs:Be thicknesses of 7 and 3.5 nm, respectively, in which AFM IEC is very clearly realized.

2. Sample preparation

The growth of GaMnAs/GaAs:Be multilayer structures used in this study was conducted on semi-insulating (001) GaAs substrates in a Riber 32 R&D MBE machine equipped with elemental sources of Ga, As, Mn and Be in the chamber. Prior to the deposition of the Mn-containing GaMnAs layer, we grew a 450 nm GaAs buffer layer at 590 °C (i.e. under normal

GaAs growth conditions). The substrate was then cooled down to 250 °C for the growth of low-temperature (LT) GaAs, usually to a thickness of 3 nm, followed by $Ga_{1-x}Mn_xAs$ and GaAs:Be multilayer structures. The As_2:Ga beam equivalent pressure ratio of 20 : 1 was used. During the growth process, the surface quality of the samples was monitored by reflection high-energy electron diffraction, which showed a (1×1) surface reconstruction for LT-GaAs, and a (2×1) reconstruction for GaMnAs. The concentrations of Mn and Be were controlled by their respective cell temperatures. A number of GaMnAs/GaAs:Be multilayer structures were prepared, with varying structural parameters such as the composition of Mn in the GaMnAs layer, the thickness of non-magnetic GaAs:Be spacers and the number of multilayers. The Mn concentrations in the GaMnAs layer and Be doping levels in the GaAs spacer were estimated from x-ray diffraction and Hall measurements, respectively, performed on the control GaMnAs and GaAs:Be epilayers grown under the same conditions as the multilayers. For structural characterization of the $[GaMnAs/GaAs:Be]_{10}$ multilayer, we carried out x-ray diffraction (XRD) measurements, which clearly show satellite peaks corresponding to the period of the multilayer. The period calculated from the satellite peaks is 10.4 nm, consistent with the neutron reflectivity measurement shown in [15]. The strong intensity and well-defined width of the satellite peaks indicate high quality of the multilayer system with uniform periodicity.

The transport measurements were performed on Hall bars patterned by photolithography and chemical wet etching on the multilayer films. The size of the Hall bar was typically $300 \times 1500\,\mu$m, with the long dimension of the bar aligned along the $[1\bar{1}0]$ direction. Ohmic contacts were obtained by bonding Au wires to the sample surface with indium. MR measurements were taken using a sample holder such that a magnetic field could be applied in the plane of the sample at an arbitrary azimuthal angle φ_H, where $[1\bar{1}0]$ is measured counterclockwise from the crystallographic direction (i.e. from the current direction) in the (001) plane.

3. Results and discussion

Figure 1(a) shows MR data obtained at 35 K during magnetization reversal with the applied magnetic field oriented in the [110] direction. The curved arrows indicate the directions of the field sweep, and the solid (blue) and open (red) circles represent the data obtained during the down-scan (i.e. field sweep from positive saturation to negative saturation) and the up-scan (i.e. field sweep from negative saturation to positive saturation) of the field, respectively. In discussing these and other data, we will refer to the process of increasing the field in either direction (which eventually aligns the magnetization of all GaMnAs layers in parallel) as the ‘saturation’ process or sweep; and we will refer to the process of recovering the initial anti-parallel (AFM) configuration by reducing the field to zero as the ‘restoring’ process. In addition to the basic GMR-like effect, we now see many clearly resolved transition steps in both the saturation and the restoring sweeps.

One could at first glance suspect that the multiple transition steps we observe are caused by unintended variations of magnetic properties between individual GaMnAs layers that could give rise to different coercive fields in the different layers comprising the superlattice (SL), thus causing their magnetizations to ‘flip’ at different fields. However, an absence of noticeable fluctuations between the GaMnAs layers in SLs of this type was confirmed in our earlier studies, in which a total of eight multilayer samples consisting of ten GaMnAs layers of varying thickness and prepared under the same growth conditions were investigated [15, 19]. When the interlayer coupling in such SLs is FM (which occurs, e.g. when the non-magnetic GaAs ‘spacer’

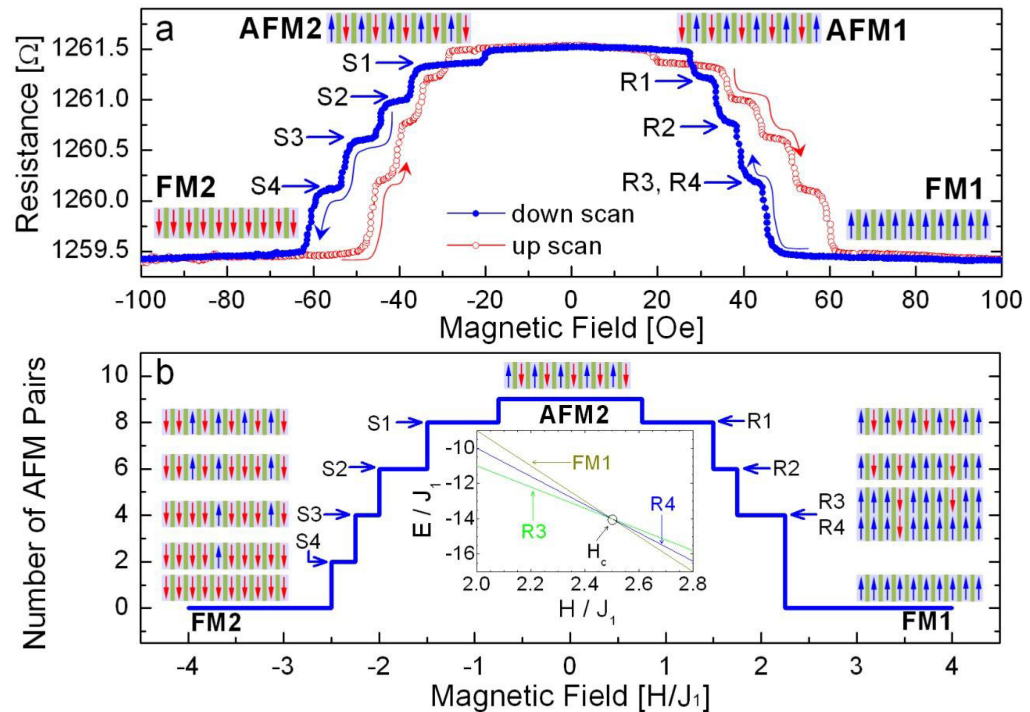

Figure 1. The process of magnetization reversal in the $[GaMnAs/GaAs:Be]_{10}$ multilayer system. (a) MR is measured at 35 K as the field is cycled between −100 and 100 Oe. The down- and up-scans, shown by solid (blue) and open (red) circles, respectively, have a completely symmetrical behavior. Two types of fully AFM spin configurations between the GaMnAs layers, AFM1 and AFM2, can be realized at zero field, as shown schematically by the vertical arrows. Each field scan (down or up) contains a four-step restoring process and a five-step saturation process, with resistance plateaus marked as R1–R4 and S1–S4. (b) The number of pairs with AFM alignment between adjacent GaMnAs layers in the multilayer is obtained by minimizing the IEC energy given by equation (1) during the down-scan of the field. The field is scaled in terms of the NN IEC strength J_1. The reversal process determined from calculation using equation (1) clearly shows a four-step restoring and a five-step saturation process, similar to that observed in the MR experiment shown in the upper panel. The crossing of the calculated energies for the R3, R4 and FM1 states is shown in the inset. The spin configuration corresponding to each plateau in the field scan is indicated schematically by vertical arrows.

layers are not doped), one observes a single abrupt transition in the magnetization reversal at LT (see figures 1 and 2 of [19]), indicating that the magnetic properties of all GaMnAs layers in each of the multilayer systems are very nearly identical. This is in sharp contrast with the very extended field range over which the magnetization of the SL discussed in the present paper is seen to reverse (by a series of magnetization flips occurring over 40 Oe between the first and the last flip). Other characteristics observed in the present system, such as the remarkable regularity of field increments at which transition steps occur during this reversal, and the difference in the

sequence of transition steps in the saturation (five steps) and restoring field sweeps (four steps) seen in figure 1, cannot be explained by an accidental variation in the properties of the magnetic GaMnAs layers comprising the SL. We must therefore rule out that possibility.

It is remarkable that the number of transition steps (five) which appear in the saturation process exactly matches the number of GaMnAs layers whose magnetization is initially aligned opposite to the direction of the applied field in the AFM alignment of the multilayer at zero field. This implies that the magnetizations of those GaMnAs layers are reversed one by one as the field increases toward saturation, as shown in figure 1(a). When the magnetic multilayer is cooled below T_C in the absence of an external field, a system consisting of ten AFM-coupled GaMnAs layers can be thought of as forming two types of anti-parallel spin configurations, AFM1 ($\downarrow\uparrow\cdots\downarrow\uparrow$) or AFM2 ($\uparrow\downarrow\cdots\uparrow\downarrow$). This idea is shown schematically in figure 1 for $H = 0$, in which arrows indicate the directions of magnetization, and the progression of the arrows from left to right corresponds to the order of the GaMnAs layers from the bottom to the top of the multilayer.

Although it is obvious that the first transition in the saturation process corresponds to the flip of magnetization in the outermost GaMnAs layer, it is difficult to identify the sequence of transitions in the inner GaMnAs layers, since the order of such flips cannot be determined by considering NN IEC alone, but must involve additional interaction terms that differentiate the strengths of IEC acting on specific interior GaMnAs layers. The most likely interaction for removing the energy degeneracy of magnetization alignments of the interior GaMnAs layers determined by NN AFM IEC is the NNN IEC. As already mentioned, this process is likely to come into play in the present case, since the Fermi wavelength of our GaMnAs samples is about 4 nm long [17, 19].

Recently, a microscopic calculation was performed to obtain the relative strength of the NNN IEC with respect to that of the NN IEC by evaluating the magnitude of spin torque between NNN magnetic layers of a multilayer [29]. The results show that the strength of NNN IEC can be as much as 24% of the strength of NN IEC. This surprisingly large value of NNN IEC may be attributed to (i) the quasi-one-dimensionality and (ii) the small thickness of the layers, as follows. (i) In bulk solids, the Ruderman–Kittel–Kasuya–Yosida (RKKY)-type exchange coupling is known to decrease (on a large scale) as $1/r^3$, where r is the distance between the interacting spins. However, for a quasi-one-dimensional system, such as our multilayer sample, it was shown in [30–33] that the IEC strength between magnetic layers decreases only as $1/r^2$, i.e. much slower. (ii) The thickness of each layer in our $[\mathrm{GaMnAs/GaAs:Be}]_{10}$ multilayer system is comparable to the Fermi wavelength, and the exchange coupling does not follow the simple power-law decay.

In discussing the magnetization reversal behavior of the GaMnAs/GaAs multilayer, we focus on understanding the multiple transition step behavior—the key feature of this experiment—rather than on quantitative details of the entire hysteresis, that would of necessity include domain wall pinning and magnetic anisotropy of each GaMnAs layer. We therefore consider only IEC energy of the multilayer and formulate the IEC energy E of the multilayer in the presence of a magnetic field H by including NNN IEC contributions. For the case of a ten-period multilayer such as our $[\mathrm{GaMnAs/GaAs:Be}]_{10}$ SL, the coupling energy can then be expressed in the form

$$E = \sum_{i=1}^{9} J_1(M_i M_{i+1}) + \sum_{i=1}^{8} J_2(M_i M_{i+2}) - \sum_{i=1}^{10} H M_i, \tag{1}$$

where J_1 and J_2 are the NN and NNN IEC constants, respectively and M_i is the magnetization of the ith GaMnAs layer.

To establish the role of NNN IEC, it is useful to first calculate the magnetic field dependence of the IEC energy for various spin configurations *without* the NNN IEC contribution (i.e. without the second term in equation (1)). The results are shown in figure 2(a), and clearly illustrate the linear dependences of the coupling energies on the field for each spin configuration. The figure shows that these energy dependences have only two crossing points, corresponding to the two critical fields at which these energies have multiple degeneracies. Specifically, the first (lower) critical field corresponds to the magnetization flip of the outermost magnetic layer that was initially aligned opposite to the applied field, and the second crossing point occurs when the magnetizations of all interior magnetic layers initially aligned opposite to the field flip their orientations. Importantly, in the NN IEC scenario, this happens at a single field for all internal layers. Thus, in this scenario, only two transitions occur in both the saturation and the restoring processes, as has indeed been observed in metallic magnetic multilayers [6].

We will now include the NNN IEC in the calculation. Although we will assume the strength of NNN IEC to be $J_2 = 0.25\, J_1$ in our calculation, qualitatively similar results are obtained with other values of J_2 if the ratio J_2/J_1 is not negligibly small. The most remarkable effect of including the NNN IEC is that it removes the energy degeneracy of the second crossing point seen in the NN IEC image (i.e. that seen in figure 2(a)), as will be discussed in detail in connection with figure 2(b).

Calculation of the lowest energy state according to equation (1) shows that, as the field is swept, many transition paths with stable spin configurations may occur, with each of these paths leading to magnetization reversal with multiple intermediate states. The results of this calculation alone are not sufficient to unambiguously determine the actual spin configurations that occur in the reversal process. Fortunately, however, the experiment provides several additional conditions that narrow down the exact spin configuration corresponding to each resistance state (i.e. each step) observed during magnetization reversal. For example, it is remarkable that in going from negative to positive saturation (up-scan) and vice versa (down-scan), we see exactly the same four-step restoration and five-step saturation paths as shown in figure 1(a). This perfectly symmetrical behavior of MR seen in the up- and down-scans of the field indicates that the AFM spin configuration at zero field switches from AFM1 and AFM2 (shown on top of figure 1(a)) on completing the five-step path to saturation and the four-step return (i.e. AFM1 $\rightarrow$ FM1 $\rightarrow$ AFM2 and then AFM2 $\rightarrow$ FM2 $\rightarrow$ AFM1). This experimental observation then establishes the following two constraints.

1. The system always experiences complete anti-parallel spin configuration (i.e. either AFM1 ($\downarrow\uparrow \cdots \downarrow\uparrow$) or AFM2 ($\uparrow\downarrow \cdots \uparrow\downarrow$)) at zero field as the field is scanned from saturation in one direction to saturation in the opposite direction.
2. The anti-parallel spin configuration at zero field always switches between AFM1 ($\downarrow\uparrow \cdots \downarrow\uparrow$) and AFM2 ($\uparrow\downarrow \cdots \uparrow\downarrow$) when the system is restored after experiencing a five-step saturation process.

Furthermore, the fact that our MR measurements are performed in the current in-plane configuration automatically identifies the location of the first transition; i.e. whether it occurs in the bottom or the top GaMnAs layer of the SL, since the current flow in this configuration will be systematically less sensitive to magnetization changes in GaMnAs layers located away from the surface of the SL (i.e. from the contacts to the sample). This leads to the third constraint.

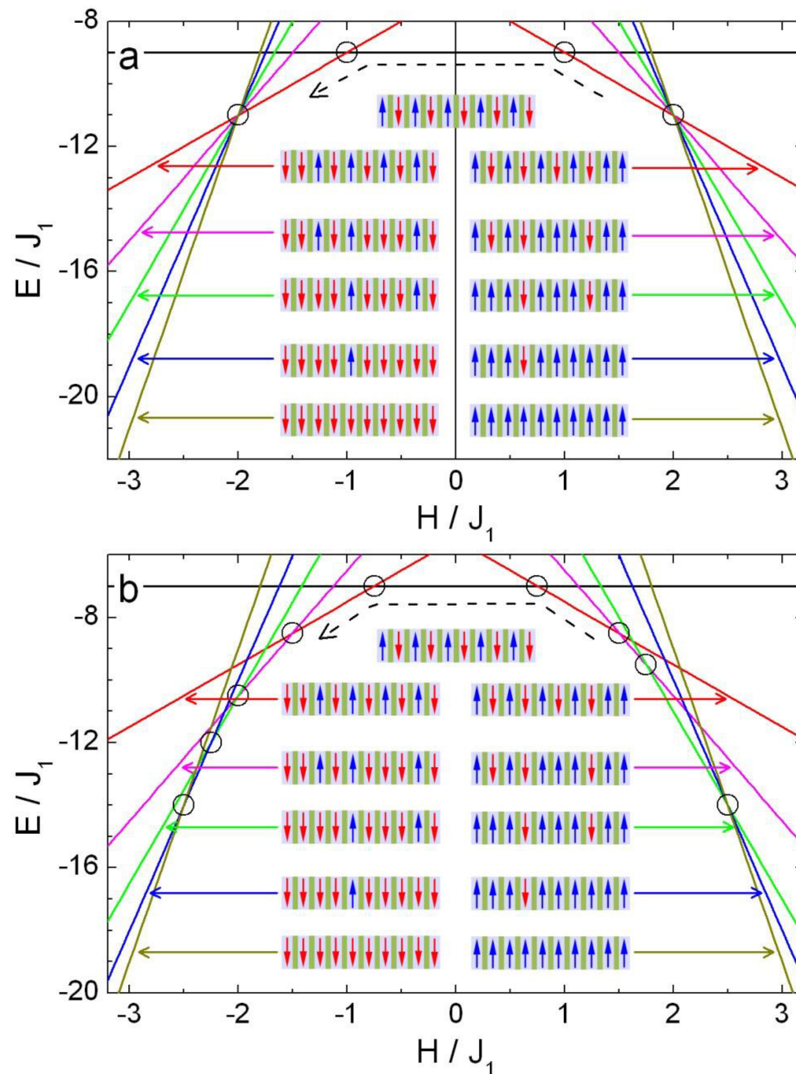

Figure 2. Calculated magnetic field dependence of energies for different spin configurations in a ten-period multilayer. (a) The upper panel shows the calculation with only NN IEC included. As indicated by the circles, only two crossing points are present for each field sweep direction. Note that in this case, many spin configurations involving inner GaMnAs layers are degenerate in energy, and that the spin configurations indicated by the vertical arrows show only one representative configuration. (b) The lower panel shows energies calculated with both NN and NNN IEC included. The specific spin configurations are determined from the three experimental constraints, as explained in the text. The results are shown only for the down-sweep of the field (i.e. from positive field saturation to negative field saturation). The results clearly show four and five crossing points, corresponding to the four-step restoring and the five-step saturation processes, respectively, as seen in the MR experiments. The dotted arrow indicates the sweeping direction of the field (down-sweep).

3. The change of resistance (measured by the voltage drop) will be the smallest for the flip of magnetization in the GaMnAs layer at the bottom of the structure.

Satisfying these three conditions uniquely determines the sequence of spin configurations (from among many possible sequences) in the course of magnetization reversal. The magnetic field dependences of energies for the resulting spin configurations for the down-scan case are shown in figure 2(b). The most interesting feature of figure 2(b) is the splitting of the second crossing point in figure 2(a) (i.e. that obtained by considering only the NN IEC) into many different crossing points. Now four and five crossing points appear in the restoring and the saturation process, respectively (as indeed seen in the data in figure 1(a)) each crossing point corresponding to a flip of magnetization in a particular GaMnAs layer.

Since the value of MR in the magnetic multilayer is a reflection of electron scattering between neighboring anti-parallel magnetic layers, we count the number of anti-parallel neighboring layer pairs occurring in the different spin configurations as the magnetization is being reversed, and plot the calculated field dependence of this number in figure 1(b) for comparison with the MR experiment. As in the case of figure 2(b), for clarity, we only plot the results for the down-scan, i.e. FM1 → AFM2 → FM2. The magnetization alignments within the structure that lead to each resistance state during the field scans are also schematically shown in figure 1(b). As one can see, the magnetization reversal path obtained by calculating the lowest coupling energy with the three experimental constraints taken into account reproduces the observed four-step restoration and the five-step saturation processes. This implies that the obtained sequence of spin configurations corresponds to the sequence of resistance states observed in the field sweeps. Since this sequence of spin configurations during magnetization reversal is obtained by considering NNN IEC, these results serve to underscore that the NNN interaction is the key factor for understanding the details of magnetization reversal in FM semiconductor multilayers such as our $[\mathrm{GaMnAs/GaAs{:}Be}]_{10}$ SL.

It is interesting to note that the restoring process (from saturation to full AFM order) undergoes a four-step transition sequence, in contrast to the five steps that we observe when progressing from full AFM order to full FM saturation. Although this is at first glance quite surprising, it can be also understood from the results of calculation shown in the inset in figure 1(b), where the field dependence of magnetic energies is plotted for the three spin configuration states (i.e. ↑↑↑↑↑↑↑↑↑↑, ↑↑↑↑↑↑↓↑↑↑ and ↑↑↓↑↑↑↓↑↑↑; designated in the figure as FM1, R4 and R3, respectively). A completely parallel configuration has the lowest energy in the region of magnetic fields larger than the field at which the FM1, R4 and R3 states have the same energy, which we designate as H_c.

Surprisingly, as the field is reduced below H_c, the magnetization configuration with two anti-parallel layers (R3) acquires a lower energy than the configuration with one anti-parallel layer (R4), even though R3 is magnetically further from FM1. Thus, the system makes a transition at H_c directly from a completely parallel configuration, FM1, to the configuration with two anti-parallel layers, R3. That is, the state with only one anti-parallel layer simply does not occur during restoration, so that this simultaneous flip of magnetization in two GaMnAs layers at the beginning of the restoring process thus results in the four-step restoring sequence, as observed in the experiment.

The four-step transition, however, occurs not only in the restoring process, but also in the saturation process when the saturation is carried out after restoration without changing the field direction, as shown with open triangles in figure 3. The three stable resistance states of the second saturation, marked as SS1, SS2 and SS3, exactly match the states in the restoring process,

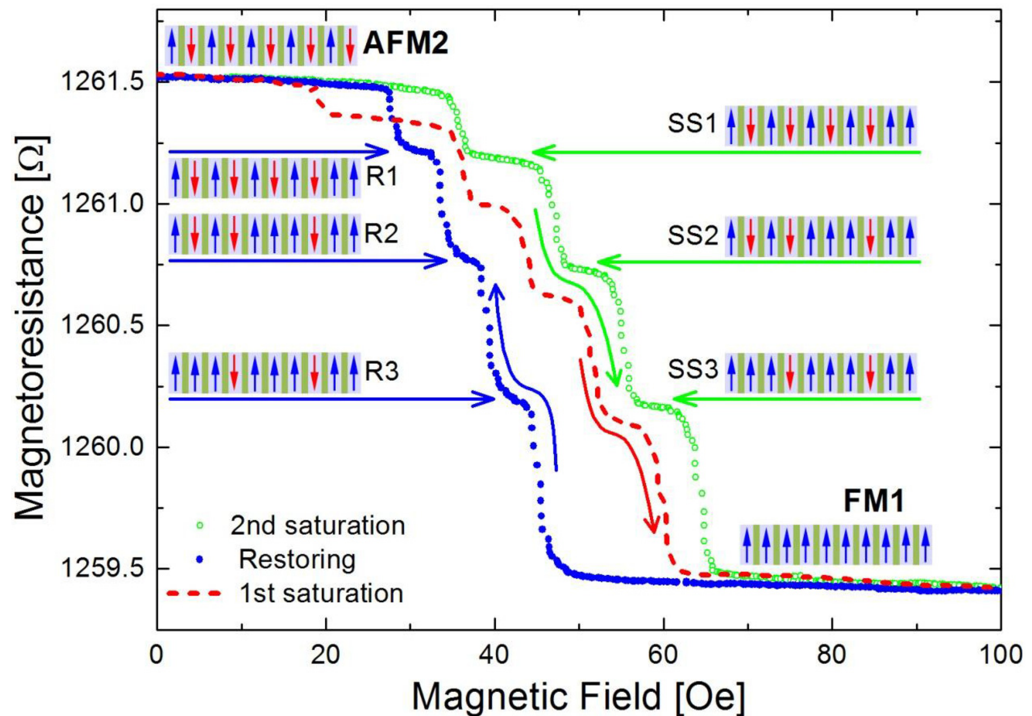

Figure 3. MR hysteresis loop obtained by cycling the positive field from saturation to restoration and back again. The dotted line (red), solid circles (blue) and open circles (green) represent data from the initial saturation, restoration and second saturation sweeps, respectively. The states realized in the second saturation process are marked as SS1–SS3, and the corresponding spin configurations are schematically shown in the figure. Unlike the initial five-step saturation process, in which the first transition corresponds to the magnetization flip of the bottom GaMnAs layer, the second saturation is a four-step process, in which the first transition corresponds to the magnetization flip of the top GaMnAs layer. Both the restoration and the second saturation are four-step processes, and exhibit identical spin configurations in reverse order.

indicating that the second saturation takes place via the same sequence of spin configurations that occurred in the restoring process; i.e. the AFM2 → FM1 and FM1 → AFM2 processes trace identical spin configurations in the reverse order.

4. Conclusions

Finally, the explanation of the various transition patterns (such as the number of steps during a given reversal process and the spin configuration of each state) is made possible in terms of the contributions of NNN IEC, which is estimated to have an approximate strength of $J_2 = 0.25\ J_1$. This contribution of NNN IEC is quite pronounced in GaMnAs/GaAs:Be multilayers because of the long range character of IEC in this semiconductor-based system, thus providing a powerful tool for investigating higher order IEC effects by experiment. We hope that this direct detection of NNN IEC in our multilayer will stimulate investigation of higher order IEC effects in other

magnetic multilayer systems. Indeed, a study on the Co/Cu/Co/Cu_{cap} system has already shown that the IEC between two Co layers depends on the thickness of the Cu capping layer [34]. Such non-magnetic capping-layer dependence of IEC suggests the possibility of NNN IEC in multilayers consisting of more than three magnetic/non-magnetic pairs. Furthermore, the presence of NNN IEC in a magnetic multilayer structure also opens a new opportunity for realizing multiple stable states that can be used for multinary information storage and/or logic devices, in which spin configurations established by IEC are controlled via electrical methods, such as injecting charge carriers into the non-magnetic spacers of the multilayer structure.

Acknowledgments

The authors thank Xiang Li for his help with XRD measurements and XRD simulation. This research was supported by the Converging Research Center Program through the Ministry of Science, ICT and Future Planning (2013K000311); by the Basic Science Research Program through the National Research Foundation of Korea (NRF) funded by the Ministry of Science, ICT and Future Planning (2013R1A1A2004505) and by the National Science Foundation Grant (DMR10-05851). J-HH and H-WL acknowledge the financial support of the NRF (numbers 2010-0014109 and 2011-0030784).

References

[1] Grünberg P, Schreiber R, Pang Y, Brodsky M B and Sowers H 1986 *Phys. Rev. Lett.* **57** 2442–5
[2] Baibich M N, Broto J M, Fert A, Van Dau F N, Petroff F, Etienne P, Creuzet G, Friederich A and Chazelas J 1988 *Phys. Rev. Lett.* **61** 2472–5
[3] Binasch G, Grünberg P, Saurenbach F and Zinn W 1989 *Phys. Rev.* B **39** 4828–30
[4] Wolf S A, Awschalom D D, Buhrman R A, Daughton J M, von Molnár S, Roukes M L, Chtchelkanova A Y and Treger D M 2001 *Science* **294** 1488–95
[5] Unguris J, Celotta R J and Pierce D T 1991 *Phys. Rev. Lett.* **67** 140–3
[6] Bloemen P J H, van Kesteren H W, Swagten H J M and de Jonge W J M 1994 *Phys. Rev.* B **50** 13505–14
[7] Borchers J A, Dura J A, Unguris J, Tulchinsky D, Kelley M H, Majkrzak C F, Hsu S Y, Loloee R, Pratt W P Jr and Bass J 1999 *Phys. Rev. Lett.* **82** 2796–9
[8] Kępa H, Le V K, Brown C M, Sawicki M, Furdyna J K, Giebultowicz T M and Dietl T 2003 *Phys. Rev. Lett.* **91** 87205
[9] Rhyne J J, Lin J, Furdyna J K and Giebultowicz T M 1998 *J. Magn. Magn. Mater.* **177–181** 1195–6
[10] Parkin S S P 1991 *Phys. Rev. Lett.* **67** 3598–601
[11] Parkin S S P, More N and Roche K P 1990 *Phys. Rev. Lett.* **64** 2304–7
[12] Lavrijsen R, Fernández-Pacheco A, Petit D, Mansell R, Lee J H and Cowburn R P 2012 *Appl. Phys. Lett.* **100** 052411
[13] Fernández-Pacheco A, Petit D, Mansell R, Lavrijsen R, Lee J and Cowburn R 2012 *Phys. Rev.* B **86** 104422
[14] Lavrijsen R, Lee J-H, Fernández-Pacheco A, Petit D C M C, Mansell R and Cowburn R P 2013 *Nature* **493** 647–50
[15] Chung J-H H, Chung S J, Lee S, Kirby B J, Borchers J A, Cho Y J, Liu X and Furdyna J K 2008 *Phys. Rev. Lett.* **101** 237202
[16] Chung J-H, Song Y-S, Yoo T, Chung S J, Lee S, Kirby B J, Liu X and Furdyna J K 2011 *J. Appl. Phys.* **110** 013912
[17] Leiner J, Lee H, Yoo T, Lee S, Kirby B J, Tivakornsasithorn K, Liu X, Furdyna J K and Dobrowolska M 2010 *Phys. Rev.* B **82** 195205

[18] Leiner J, Tivakornsasithorn K, Liu X, Furdyna J K, Dobrowolska M, Kirby B J, Lee H, Yoo T and Lee S 2011 *J. Appl. Phys.* **109** 07C307

[19] Chung S, Lee S, Chung J-H H, Yoo T, Lee H, Kirby B, Liu X and Furdyna J K 2010 *Phys. Rev.* B **82** 054420

[20] Dietl T, Ohno H, Matsukura F, Cibert J and Ferrand D 2000 *Science* **287** 1019–22

[21] Dietl T, Ohno H and Matsukura F 2001 *Phys. Rev.* B **63** 195205

[22] Chiba D, Akiba N, Matsukura F, Ohno Y and Ohno H 2000 *Appl. Phys. Lett.* **77** 1873–5

[23] Kirby B J, Borchers J A, Liu X, Ge Z, Cho Y J, Dobrowolska M and Furdyna J K 2007 *Phys. Rev.* B **76** 205316

[24] Kępa H, Kutner-Pielaszek J, Twardowski A, Majkrzak C F, Sadowski J, Story T and Giebultowicz T M 2001 *Phys. Rev.* B **64** 121302

[25] Akiba N, Matsukura F, Shen A, Ohno Y, Ohno H, Oiwa A, Katsumoto S and Iye Y 1998 *Appl. Phys. Lett.* **73** 2122–4

[26] Sankowski P and Kacman P 2005 *Phys. Rev.* B **71** 201303

[27] Giddings A D, Jungwirth T and Gallagher B L 2008 *Phys. Rev.* B **78** 165312

[28] Szałowski K and Balcerzak T 2009 *Phys. Rev.* B **79** 214430

[29] Han J-H and Lee H-W 2012 *Phys. Rev.* B **86** 174426

[30] Kittel C 1969 *Introduction to Solid State Physics* vol 22, ed F Seitz, D Turnbull and H Ehrenreich (New York: Academic) pp 1–26

[31] Yafet Y 1987 *Phys. Rev.* B **36** 3948–9

[32] Bruno P and Chappert C 1991 *Phys. Rev. Lett.* **67** 1602–5

[33] Bruno P and Chappert C 1992 *Phys. Rev.* B **46** 261–70

[34] de Vries J J, Schudelaro A A P, Jungblut R, Bloemen P J H, Reinders A, Kohlhepp J, Coehoorn R and de Jonge W J M 1995 *Phys. Rev. Lett.* **75** 4306–9